

## RESEARCH ARTICLE SUMMARY

## STRUCTURAL BIOLOGY

# Structure of the mitochondrial inner membrane AAA<sup>+</sup> protease YME1 gives insight into substrate processing

Cristina Puchades, Anthony J. Rampello, Mia Shin, Christopher J. Giuliano, R. Luke Wiseman, Steven E. Glynn,\* Gabriel C. Lander\*

**INTRODUCTION:** Protein quality control is essential for mitochondrial function, and imbalances in this regulation are associated with numerous human diseases. YME1L is a hexameric AAA<sup>+</sup> protease in the inner membrane (IM) that controls maintenance of the electron transport chain, protein import, lipid synthesis, and mitochondrial morphology. Every YME1L subunit contains an adenosine triphosphatase (ATPase) and a peptidase domain, which reside in the intermembrane space, tethered to the IM by a membrane helix. Protein substrates undergo adenosine triphosphate (ATP)-driven translocation through a central pore into a proteolytic chamber by a mechanism that is likely to be conserved in other AAA<sup>+</sup> proteases.

**RATIONALE:** A compelling question is how YME1L couples ATP hydrolysis to processive substrate translocation. We sought to understand this mechanism by determining a near-atomic resolution cryo-electron microscopy (cryo-EM) structure of a solubilized form of the yeast homolog, YME1. By precisely visualizing how the nucleotide state of YME1 subunits allosterically controls their interaction with a translocating protein substrate, we can understand how cycles of nucleotide hydrolysis can drive stepwise translocation of protein substrates for degradation.

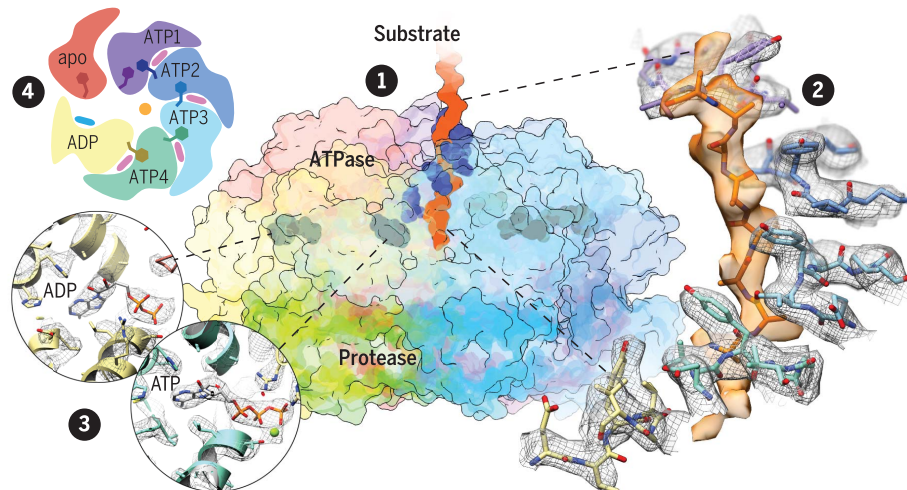
**RESULTS:** Our ~3.4 Å resolution structure shows that YME1 assembles into two stacked rings, with an asymmetric spiral staircase of

ATPase domains atop a planar protease ring. Tyrosine residues in two conserved central ATPase pore loops grasp an unfolded 10-amino acid peptide and direct it toward a negatively charged proteolytic chamber. The four central subunits in the staircase bind ATP and intercalate their pore loop tyrosines with the substrate backbone in a configuration compatible with sequence-independent translocation. The lowest “posthydrolysis” subunit contains an adenosine diphosphate (ADP)-like EM density and only interacts modestly with the substrate, whereas the top apo-like step subunit does not contain well-resolved nucleotide density and is disengaged from both the substrate and the ATPase ring.

Bound ATP is sensed by the adjacent promoter via two arginine fingers and an inter-subunit signaling (ISS) motif that bridges the subunits across the nucleotide-binding pocket. Attachment of the ISS positions the pore loop tyrosines of the ATP-bound subunit to tightly grasp the substrate. Loss of the  $\gamma$ -phosphate releases the arginine fingers, retracting the ISS and repositioning the pore loops away from the substrate. The absence of nucleotide in the step subunit breaks coordination on both sides and sequesters the pore loops into helices away from the substrate. A glycine residue in the interdomain linker is required to accommodate large movements of the ATPase domains within the spiral staircase.

**CONCLUSION:** This structure of a substrate-bound single-polypeptide AAA<sup>+</sup> protease allows us to define a tightly coordinated sequential ATP hydrolysis cycle. Hydrolysis in the lowest ATP-bound subunit abolishes coordination by the adjacent arginine fingers and ISS, repositioning the now posthydrolysis subunit to the lowest position of the staircase, which, in turn, triggers hydrolysis in the next-lowest ATP-bound subunit. Loss of coordination on both sides of the ADP-bound subunit breaks substrate interaction and displaces the subunit from the hexamer, where it can release ADP and rebind ATP at the top of the staircase. Iteration of this cycle drives stepwise translocation of the substrate into the proteolytic chamber. The high degree of structural conservation between YME1 and the 26S proteasome suggests that this mechanism may be conserved across ATP-driven proteases. ■

The list of author affiliations is available in the full article online.  
\*Corresponding author. Email: glander@scripps.edu (G.C.L.); steven.glynn@stonybrook.edu (S.E.G.)  
Cite this article as C. Puchades et al., *Science* 358, eaao0464 (2017). DOI: 10.1126/science.aao0464



**Cryo-EM structure of AAA<sup>+</sup> protease YME1 sheds light on the mechanism of substrate translocation.** (1) A semitransparent surface representation shows how the asymmetric ATPase staircase is positioned above a planar C<sub>6</sub>-symmetric protease ring. Substrate (orange) surrounded by pore loop 1 tyrosines is shown in blue. Nucleotides are shown as gray densities. (2) A close-up view of the cryo-EM density reveals a spiral staircase organization with tyrosines intercalating into the substrate. (3) The nucleotide state could be identified for each subunit. (4) A cartoon representation of the YME1 ATPase hexamer depicts the asymmetric organization of the subunits surrounding the substrate. The ISS motif (represented as a Phe residue) protrudes into the nucleotide-binding pocket of the neighboring subunit only in the presence of ATP.

## RESEARCH ARTICLE

## STRUCTURAL BIOLOGY

# Structure of the mitochondrial inner membrane AAA+ protease YME1 gives insight into substrate processing

Cristina Puchades,<sup>1,2</sup> Anthony J. Rampello,<sup>3</sup> Mia Shin,<sup>1,2</sup> Christopher J. Giuliano,<sup>3</sup>  
R. Luke Wiseman,<sup>2</sup> Steven E. Glynn,<sup>3\*</sup> Gabriel C. Lander<sup>1\*</sup>

We present an atomic model of a substrate-bound inner mitochondrial membrane AAA+ quality control protease in yeast, YME1. Our ~3.4-angstrom cryo-electron microscopy structure reveals how the adenosine triphosphatases (ATPases) form a closed spiral staircase encircling an unfolded substrate, directing it toward the flat, symmetric protease ring. Three coexisting nucleotide states allosterically induce distinct positioning of tyrosines in the central channel, resulting in substrate engagement and translocation to the negatively charged proteolytic chamber. This tight coordination by a network of conserved residues defines a sequential, around-the-ring adenosine triphosphate hydrolysis cycle that results in stepwise substrate translocation. A hingelike linker accommodates the large-scale nucleotide-driven motions of the ATPase spiral relative to the planar proteolytic base. The translocation mechanism is likely conserved for other AAA+ ATPases.

## INTRODUCTION

The regulation of mitochondrial protein quality control is essential for mitochondrial function and cellular survival. Imbalances are associated with a variety of human diseases, including many neurological and cardiovascular disorders (1–3). Most of the mitochondrial proteome cannot be accessed by the cytosolic ubiquitin/proteasome pathways; thus, mitochondrial protein quality control is primarily controlled by a network of proteases that degrade damaged or misfolded proteins (4, 5), such as the human AAA+ protease YME1L in the inner membrane (IM). YME1L is involved in nearly all aspects of mitochondrial biology, including regulation of the electron transport chain, protein import, lipid synthesis, and mitochondrial morphology (6–9). Stress-induced reductions in YME1L activity severely disrupt mitochondrial function and increase cellular stress sensitivity both in vitro and in vivo (10–12). Similarly, genetic ablation of *Yme1l1* in mice is embryonic lethal and conditional deletion in adult cardiomyocytes causes heart failure and premature death (13). Furthermore, homozygous mutation of *Yme1l1* causes mitochondrialopathy with optic nerve atrophy in humans (14).

Despite its crucial function, a lack of structural information for YME1L or its homologs in

other eukaryotes, or even any of the other mitochondrial IM AAA+ proteases (such as AFG3L2), hinders our understanding of these mitochondrial quality control machines. Unlike the proteolysis-associated AAA+ unfoldases found in the eukaryotic cytoplasm, which comprise only adenosine triphosphatase (ATPase) domains and interact with separate proteolytic complexes (that is, the 20S core particle), mitochondrial IM AAA+ proteases contain both ATPase and protease domains on a single polypeptide, separated by a short linker region. In YME1L, the AAA+ ATPase domain and M41 peptidase domains reside in the mitochondrial intermembrane space, tethered to the IM by a single-pass membrane helix (Fig. 1, A and B). YME1L is evolutionarily related to bacterial FtsH, and the catalytic domains exhibit a high degree of conservation across all eukaryotes (1, 15). The catalytic domains of the yeast homolog, YME1, share 54% sequence identity with the human homologs, and expressing human *Yme1l1* in a *yme1-1*-deficient yeast restores mitochondrial function, indicating comparable activities and substrate profiles (16).

A recently engineered soluble construct of yeast YME1, <sup>hex</sup>YME1, comprising the AAA+ ATPase and protease domains assembled into active oligomers by fusion to a coiled-coil hexamerizing domain, exhibits high ATPase and proteolytic activity, as well as biologically relevant substrate specificity (17, 18). Here, we used a <sup>hex</sup>YME1 variant containing an E381Q Walker B mutant (<sup>hex</sup>YME1<sup>WB</sup>) that limits adenosine triphosphate (ATP) hydrolysis to enable structural determination of this ATP-dependent protease by cryo-electron microscopy (cryo-EM) (Fig. 1 and figs. S1 and S2). We present an atomic model of a

mitochondrial IM AAA+ protease to reveal the allosteric mechanism linking ATP hydrolysis to substrate translocation in YME1.

## Quaternary organization of the substrate-engaged YME1 AAA+ protease

The <sup>hex</sup>YME1<sup>WB</sup> hexamer was solved in the presence of saturating amounts of ATP (1 mM). The cryo-EM reconstruction was estimated to have an overall resolution of ~3.4 Å, with the best-resolved regions at ~3.2 Å, providing a near-atomic resolution view of the homohexameric nucleotide-bound <sup>hex</sup>YME1<sup>WB</sup> complex (Fig. 1, fig. S2, and table S1). Our structure describes how the catalytic domains assemble into two stacked rings, with an asymmetric spiral staircase comprising the ATPase domains atop a planar, C6-symmetric protease ring (Fig. 1, A and B). Together, the ATPase and protease rings enclose a negatively charged proteolytic chamber encircled by the interdomain linker (Fig. 1, A and B, and fig. S3A).

Previous crystal structures of the bacterial FtsH in adenosine diphosphate (ADP)-bound and nucleotide-free conformations contained ATPase domains organized into hexameric rings with two-, three-, and sixfold symmetry (19–21). Although the topological organization of the YME1 protomer closely resembles that of FtsH (Fig. 1D), our structure reveals a distinctly different quaternary organization. Instead of a symmetric organization of the AAA+ domains, the YME1 AAA+ domains assemble into a spiral staircase, with the ATPases progressively rotated and translated with respect to one another, similar to the organization observed for numerous other AAA+ unfoldases, including the functionally related 26S proteasome ATPase (Fig. 1, A and C) (22–26). In our YME1 structure, a “step” subunit (red throughout Fig. 1) connects the lowest and highest positions of the staircase spiral (yellow and purple in Fig. 1, B and C, respectively), characteristic of closed-ring, type I AAA ATPases (23, 25, 27). Because of the known positional variability of this step subunit, focused three-dimensional (3D) classification of this protomer was used to enable confident atomic modeling in this region (fig. S2, D to G). Despite many similarities to previously determined AAA ATPases, our YME1 structure is distinct in that it describes a spiraling AAA+ protease wherein the ATPase and protease domains are contained on the same polypeptide chain.

The central pore of the ATPase spiral staircase has a diameter of ~1.4 nm, sufficient to accommodate an unfolded peptide (Fig. 1B). Surprisingly, we discovered an additional density within the pore, oriented at a 28° angle relative to the hexameric axial axis, into which an unfolded 10-amino acid peptide could be modeled (Fig. 1, A, B, and D, and movie S1). We conclude that this density represents a substrate peptide that is trapped in the process of translocation through the YME1 pore. Although the origin of this peptide is unclear, it is possible that the presence of a substrate polypeptide stabilizes the observed conformation, because the only subset of YME1 complexes contributing to the high-resolution structure contained this substrate density. Cryo-EM

<sup>1</sup>Department of Integrative Structural and Computational Biology, The Scripps Research Institute HZ 175, 10550 North Torrey Pines Road, La Jolla, CA 92037, USA. <sup>2</sup>Department of Molecular Medicine, The Scripps Research Institute, La Jolla, CA 92037, USA. <sup>3</sup>Department of Biochemistry and Cell Biology, Stony Brook University, 450 Life Sciences Building, Stony Brook, NY 11794, USA.

\*Corresponding author. Email: glander@scripps.edu (G.C.L.); steven.glynn@stonybrook.edu (S.E.G.)

reconstructions of other ATPases in similar asymmetric spiraling configurations also revealed substrate density in the central pores (23, 24, 28), suggesting that substrate binding may induce this conformation. The presence of this substrate and the resolution of our structure provide an opportunity to define how YME1 translocates substrates.

### YME1 ATPase domains engage substrates through a double spiral staircase of tyrosines

A conserved aromatic-hydrophobic motif (typically Tyr/Phe-Val) in the central pore loop 1 is found across AAA+ ATPases, and numerous studies show direct involvement of the motif in AAA+-dependent unfolding and translocation (29–34). In YME1, mutation of the conserved aromatic residue (Y354) impairs substrate degradation, confirming the importance of this residue (35). Notably, we see direct association of Y354 with the translocating substrate in our YME1 complex, with the Y354 residues adopting a spiral staircase organization that mirrors the global architecture of the AAA+ domains (Figs. 1E and 2A). The Y354 residues show three distinct modes of interaction with the translocating substrate, relative to their position in the staircase architecture. The central four Y354 residues are intercalated into the substrate, with each Y354 positioned between substrate side chains to engage the substrate backbone in a zipperlike configuration (Fig. 2A and fig. S4), a nonspecific mode of interaction that is compatible with sequence-independent substrate translocation essential for the function of YME1. However, the lowest Y354 (Fig. 2A, yellow) shows a less-extensive interaction with the substrate, and Y354 of the step subunit, whose pore loop 1 adopts the topmost position within the Tyr staircase (Fig. 2A, red), is completely disengaged from the substrate. Thus, the positioning of the specific ATPases within the spiral staircase dictates the engagement of Y354 with the substrate. Additionally, our structure shows that the adjacent valine of the conserved aromatic-hydrophobic motif of pore loop 1 (V355) is directed toward the substrate side chains (Fig. 1E), in agreement with previous biochemical data implicating this residue in dictating substrate specificity for FtsH (31, 36).

Unexpectedly, we also observed that another tyrosine residue, Y396 within the pore loop 2 of the YME1 AAA+ domains, forms a second spiral arrangement surrounding the substrate at a position below the pore loop 1 staircase (Fig. 2A). The interactions between Y396 and the translocating substrate mirror those observed for the pore loop 1 Y354—the Y396 residues within the central four ATPase domains in the spiral staircase appear to interact with the substrate, whereas the Y396 residue of the lowest subunit is positioned further away from the substrate and the Y396 residue of the step subunit is completely disengaged. Although the presence of a tyrosine residue in this position is conserved across YME1 homologs, including mammalian YME1L, this

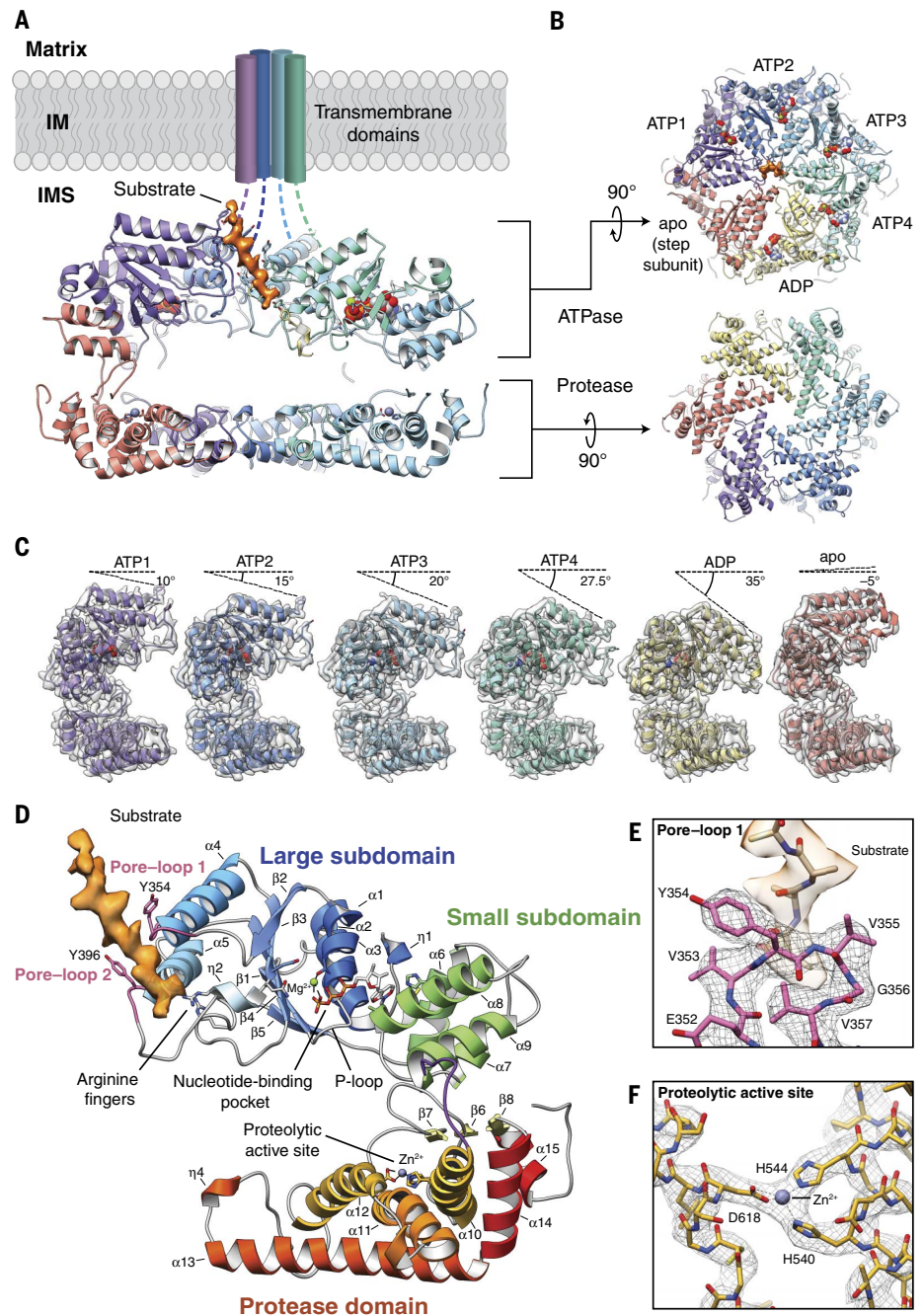


**Fig. 1. Architecture of the substrate-bound YME1 AAA+ protease.** (A) Cutaway view of the substrate-bound YME1 atomic model, with cryo-EM density for substrate colored orange. Each subunit of the homohexamer is assigned a different color, and the nucleic acids are depicted using a sphere representation in (A) to (C). (B) Views of the ATPase and protease rings, shown orthogonally to the orientation shown in (A). (C) Individual protomers shown side by side, aligned with the protease domain in the same orientation. The cryo-EM density is shown as a transparent gray isosurface, showing the quality of the reconstruction. The sequential movement of the ATPase domain relative to the protease domain is emphasized by a dashed line above each protomer, depicting the tilt of the pore loop helices relative to the horizontal protease ring. The pore loop tyrosines are visible within each of the pore loops. (D) Topological organization of the YME1 protomer showing the large and small subdomains of the ATPase domain and protease domain underneath. Notable and conserved components of the YME1 subunit are highlighted. The cryo-EM density of the substrate is shown in orange. (E) Detailed view of the pore loop 1 interactions with the substrate. The cryo-EM density of the substrate is shown as a transparent orange isosurface, along with a polyaniline model of the substrate. The cryo-EM density of the pore loop is shown as a mesh, and the atomic model shows the interaction of Y354 and V355 with the substrate. (F) Detailed view of the zinc-coordinated proteolytic active site.

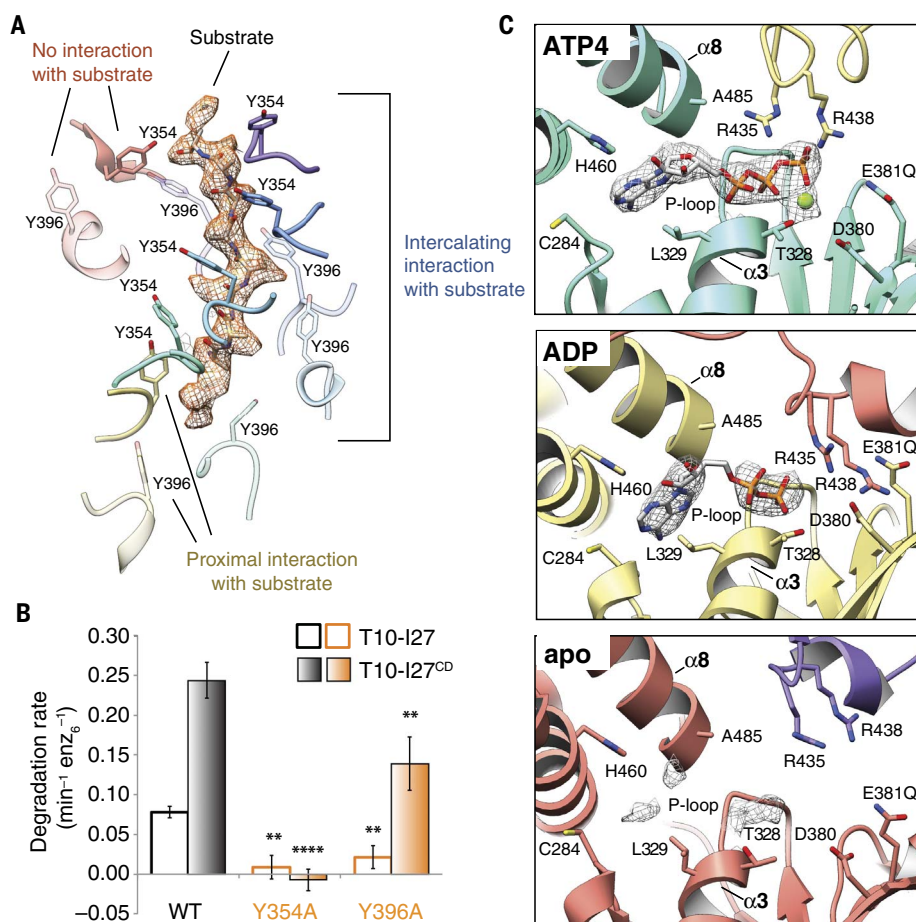


**Fig. 2. Nucleotide state correlates with pore loop conformation and substrate interaction.**

(A) Three categories of interactions are observed between the pore loop tyrosines and substrate. A polyaniline model of the substrate is shown within the cryo-EM density of the substrate, shown as orange mesh. Y354 and Y396 from pore loop 1 and pore loop 2 are rendered as solid and semitransparent, respectively. The Tyr residues from the ATP(1–4) subunits (purple, blue, cyan, and turquoise) show close, stable, intercalating interactions with the substrate, whereas those from the ADP subunit (yellow) are positioned further from the substrate, and those from the apo subunit (red) show no interaction with the substrate. (B) Effect of mutations in the conserved pore loops on substrate degradation. Initial degradation rates are shown for folded (T10-I27) and unfolded (T10-I27<sup>CD</sup>) substrates by wild-type (WT) <sup>hex</sup>YME1 and variants bearing either Y354A or Y396A substitutions. Mutation of the pore loop 1 tyrosine abolishes the degradation rate for both substrates, and mutation of the pore loop 2 tyrosine significantly diminishes the degradation rate for both substrates, consistent with an important role for both of these residues in substrate handling. Values are means of independent replicates ( $n \geq 3$ )  $\pm$  SD.  $**P \leq 0.01$ ,  $****P < 0.0001$  as calculated using Student's two-tailed  $t$  test and shown in comparison to the degradation of the identical substrate by WT <sup>hex</sup>YME1. (C) Organization of the nucleotide-binding pockets in the ATP(1–4), ADP, and apo states. Cryo-EM density corresponding to the nucleotide (or lack thereof) is shown as a gray mesh at a  $\sigma$  level of 4.0 for all states. The absence of  $\gamma$ -phosphate and magnesium ion is evident in the ADP-like state, whereas only a low level of nucleotide density is still present in the apo subunit (bottom panel). In the ATP(1–4) and ADP conformations, the adenine base is located within 4 Å of L329 and C284 of the large domain and H460 of the small domain, whereas the ribose directly interacts with the backbone of A485 from helix  $\alpha 8$  of the small domain. The arginine fingers (R435 and R438) are closely coordinated with the phosphates in the ATP(1–4) subunits but are further away in the ADP and apo subunits.

residue is not found in more distantly related mitochondrial enzymes, such as AFG3L2, or in cytosolic AAA+ proteases, such as the 26S proteasome.

To confirm that these observed pore loop interactions play a role in substrate translocation, we examined the substrate degradation activity

of <sup>hex</sup>YME1 containing point mutations in the pore loop 1 tyrosine (Y354A) or the pore loop 2 tyrosine (Y396A). The introduction of these mutations into either pore loop largely abolishes the degradation of the I27 domain of human titin bearing an N-terminal degron derived from the mitochondrial Tim10 protein (T10-I27) (Fig. 2B)

(18). The introduction of mutations in the I27 domain to destabilize the folded structure (T10-I27<sup>CD</sup>) produced a large increase in the degradation rate by wild-type <sup>hex</sup>YME1, likely resulting from the removal of the unfolding step of the degradation (37). This unfolded protein was not degraded by <sup>hex</sup>YME1 bearing the Y354A mutation, and the degradation rate of Y396A was substantially reduced compared to wild type. Together, these results demonstrate that both pore loop tyrosines are important for substrate degradation. The Y354A mutant, but not Y396A, also impaired ATP hydrolysis, suggesting allosteric coordination linking substrate interactions at the pore loop with the nucleotide-binding pocket (fig. S1B), and that substrate binding may help position the YME1 subunits for efficient ATPase activity. This was previously shown biochemically for FtsH and other AAA+ ATPases (36, 38, 39), but the mechanism of this allostery has remained elusive, prompting us to explore the relationship between the nucleotide state and the observed pore loop conformations.

### YME1 contains three coexisting nucleotide states

The resolution of our reconstruction enabled us to unambiguously define the nucleotide state for each subunit within the YME1 homohexamers. We observe three distinct nucleotide states coexisting within the structure. Four subunits in the YME1 AAA+ spiral staircase (ATP1, ATP2, ATP3, and ATP4 shown in Fig. 1B) contain a well-resolved ATP in the nucleotide-binding pocket, defined by the presence of the three phosphate residues (Fig. 2C; fig. S5, A and B; and movie S1). The lowest subunit of the spiral staircase has an ADP-like density in the nucleotide-binding pocket (ADP in Figs. 1B and 2C; fig. S5, A and B; and movie S1), whereas the binding pocket of the step subunit contains weak nucleotide density, which we refer to as “apo-like” (Fig. 2C; fig. S5, A and B; and movie S1). The presence of ADP-like density in the lowest subunit can be explained by the presence of small amounts of contaminating ADP or by low residual ATP hydrolysis in the Walker B mutant (40, 41).

These three distinct nucleotide states correlate directly with the three modes of interaction we observe between the pore loop tyrosines and the translocating substrates. The ATP-bound subunits directly engage the substrate (Figs. 1, A and B, and 2A). The ADP-bound subunit proximally associates with the substrate, and the apo-like subunit is completely disengaged. This direct correlation between nucleotide states and substrate engagement, combined with our biochemical results, suggests that nucleotide hydrolysis and release provides a mechanism to allosterically regulate the pore loop conformations and direct substrate translocation.

### The spiral staircase organization links nucleotide state to pore loop conformation

Nucleotides bind to AAA+ ATPases within a pocket formed at the interface of the large and

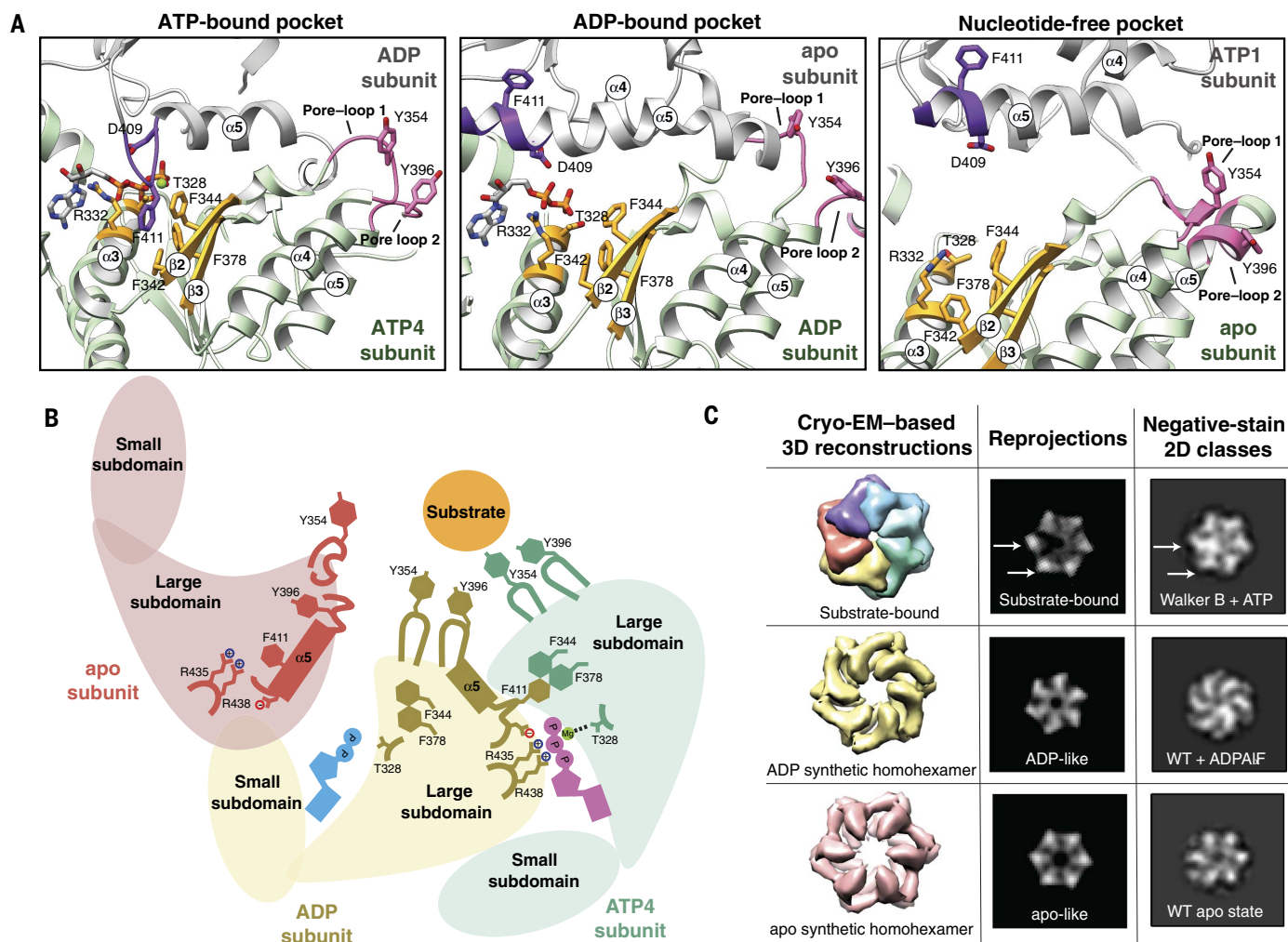


**Fig. 3. Nucleotide state causes major conformational rearrangements of the ATPase domain.**

(A) The three nucleotide state conformations were aligned to the central Phe-containing  $\beta$  sheet (colored gold) to show the major rearrangements that allosterically affect pore loop conformation. In the ATP-bound pocket, the ISS loop of the adjacent subunit (purple) extends toward the Phe-containing  $\beta$  sheet. In this conformation, the pore loops (pink) are extended toward the central pore and interact strongly with the substrate. In the ADP-bound pocket, loss of the  $\gamma$ -phosphate results in a retraction of the ISS loop from the Phe-containing  $\beta$  sheet, and the ISS loop becomes part of the  $\alpha 5$  helix of the adjacent subunit. Within the ADP-bound subunit, the  $\alpha 3$  helix moves closer to the Phe-containing  $\beta$  sheet, and the pore loop tyrosines more weakly interact with the substrate. In the nucleotide-free state, the pore

loop tyrosines are completely dissociated from the substrate and are incorporated into helices 4 and 5. (B) Cartoon representation of the nucleotide-dependent conformational changes affecting the entire ATPase domain, depicting the motions described in (A). When ATP is bound within the nucleotide pocket, the pore loop tyrosines interact strongly with the substrate. ATP hydrolysis results in a weakening of the substrate-tyrosine interactions, and loss of the nucleotide results in a complete release of the substrate. (C) Nucleotide state is shown to cause major domain rotations, because 3D structures of the substrate-bound and computationally symmetrized ADP and apo homohexamers generate distinctly different 2D projections that show structural characteristics that are similar to those in reference-free 2D classes obtained by negative-stain EM in the presence of ATP and ADPAIF<sub>x</sub> or in the absence of nucleotide.

small subdomains of one ATPase and the large subdomain of the neighboring ATPase (Fig. 2C). YME1 belongs to the P-loop subclass of ATPases, which are characterized by a conserved Walker A motif (GXXGXXGK[S/T]) in the large subdomain that directly interacts with nucleotide (42). Accordingly, backbone nitrogens of the P-loop residues G324 and G326 directly interact with the nucleotide phosphates in our YME1 structure (fig. S5B). Notably, all residues that were previously found to be crucial for nucleotide binding in YME1 (43) are involved in nucleotide interaction in our structure (Fig. 2C).

The machinery of ATP hydrolysis is highly conserved across AAA+ ATPases, simultaneously involving side chains from both the large and small ATPase domains, as well as trans-acting residues of the neighboring subunit. Within the YME1 nucleotide-binding pocket, a threonine (T328 in  $\alpha 3$  of YME1) coordinates a magnesium ion with the ATP phosphates (Figs. 2C, top, and 3A). In addition, two consecutive acidic residues (D380 and E381 in YME1  $\beta 1$ ) coordinate and activate a catalytic water molecule. The large ATPase subdomain of the neighboring protomer contributes to the coordination of the ATP  $\gamma$ -phosphate

through two conserved “arginine fingers” (R435 and R438 in YME1) (42). Furthermore, in the presence of ATP, we observe a loop (D409-G410-F411) at the C-terminal end of  $\alpha 5$  of this adjacent subdomain that bridges across the nucleotide-binding pocket, contacting the ATP-bound subunit. This loop is strictly conserved across homologs and paralogs of YME1, as well as in the ATPases of the 26S proteasome (fig. S7A). This region has been previously identified as the intersubunit signaling (ISS) motif, because mutagenesis of these residues revealed a critical role in communicating the nucleotide

state between protomers (44). In this extended conformation of the ISS motif, D409 is in close proximity to the arginine fingers, and the ISS phenylalanine (F411) packs against phenylalanine residues in  $\beta 2$  and  $\beta 3$  of the ATP-bound subunit (Fig. 3A, purple in left panel, and movie S2). These aromatic interactions position the pore loop 1 and 2 tyrosines protruding from  $\alpha 4$  and  $\alpha 5$  of the ATP-bound subunit in an orientation that is compatible with substrate engagement [Fig. 3, A (pink in left panel) and B (green), and fig. S6].

Loss of the ATP  $\gamma$ -phosphate disrupts the interprotomer coordination between the ISS motif in the apo step subunit and the nucleotide-binding pocket within the ADP-like subunit (Fig. 3, A and B, and fig. S6). This results in a twofold increase in the distance between the step subunit's arginine fingers and the ADP-like nucleotide-binding site. This reduced coordination between subunits causes the ISS motif of the apo step subunit to retract from the neighboring nucleotide-binding pocket of the ADP-bound subunit and become incorporated into the C-terminal end of a now-extended  $\alpha 5$  (Fig. 3A, purple in middle panel, and movie S2). This helical refolding of the ISS loop disrupts the aromatic interactions between F411 of the apo step subunit and the phenylalanine residues in the  $\beta 2$  and  $\beta 3$  strands of the ADP-like subunit. In the absence of the trans-acting F411 from the apo step subunit, the  $\alpha 3$  helix of the ADP-like subunit is drawn closer to the central  $\beta$  sheet, shifting T328 away from the magnesium coordination site. Together, these rearrangements reconfigure the pore loop tyrosines in the ADP subunit to orientations positioned away from the substrate [Fig. 3, A (pink in middle panel) and B (gold), and fig. S6].

In addition to precluding the interaction between F411 and the ADP-bound subunit (Fig. 3A, purple in middle panel; fig. S6; and movie S2), the lack of nucleotide in the step subunit also prevents interprotomer stabilization by a trans-acting F411 from the ATP1 subunit (Fig. 3A, purple in right panel, and fig. S6). As a result, the step subunit is disconnected from both neighboring protomers, explaining the high positional flexibility for this subunit observed in our cryo-EM reconstruction. This lack of interprotomer coordination results in an N-terminal extension of the step subunit  $\alpha 5$  helix, altering the conformation of pore loop 2 and resulting in its incorporation into the  $\alpha 5$  helix [Fig. 3, A (pink in right panel) and B]. The extension of the  $\alpha 5$  helix at both the N- and C-terminal ends results in a sequestration of the pore loop 2 Y396 from substrate interaction and simultaneously influences the conformation of the adjacent  $\alpha 4$  helix to reposition the pore loop 1 Y354 away from the substrate (fig. S6B).

Together, our results indicate that nucleotide binding and hydrolysis regulate the interactions between the pore loop tyrosine double staircase and the substrate (Fig. 3B and fig. S6). In the ATP-bound subunits, the nucleotide-binding pocket is positioned to allow hydrolysis, and although the precise trigger for hydrolysis is not

clear from the structure, it is likely that subtle changes in the position of the arginine fingers from the adjacent ADP-like subunit are required to trigger hydrolysis in the ATP4-binding site. Loss of the  $\gamma$ -phosphate induces remodeling of the nucleotide-binding pocket, which reorganizes the pore loop tyrosine residues of both the ADP-like subunit and the neighboring step subunit, dissociating these subunits from the substrate. Thus, the three nucleotide states coexisting in our substrate-bound structure suggest that the nucleotide state allosterically regulates pore loop interactions with substrates through conformational remodeling of the AAA+ ATPase domain.

### Nucleotide state coordinates major structural rearrangements within the ATPase domains

To better define the interdomain reorganizations induced by the nucleotide state, we calculated difference distance matrix plots that depict changes in distances between  $C\alpha$  atoms between one subunit and its clockwise neighbor (fig. S8A). These matrices show that the small and large subdomains undergo substantial rigid-body movements independently of each other in a nucleotide-dependent manner. The subdomains are closest to one another in the ADP-like subunit, whereas the distance is maximal in the step subunit (fig. S8A).

To investigate the role that the nucleotide state plays in directing this subdomain positioning, we structurally characterized  $^{\text{hex}}\text{YME1}^{\text{WT}}$  in the absence of nucleotide, as well as in the presence of ADPAIF<sub>x</sub>, an ATP analog known to induce ATP hydrolysis intermediate states in other AAA+ ATPases (45, 46). In both the absence of ATP and the presence of ADPAIF<sub>x</sub>, the conformational heterogeneity of the hexamer rose to a level that impeded 3D reconstructions. However, 2D analysis using negative-stain EM was sufficient to inform on the overall domain organization of these hexameric states. Reference-free 2D analyses revealed three substantively different conformations in the absence of nucleotide or in the presence of ATP and ADPAIF<sub>x</sub>, confirming that a reorganization of the protomer is associated with specific nucleotide states (Fig. 3C, right column).

To assess whether the distinct tertiary organizations represented by these 2D analyses are consistent with the nucleotide-induced rearrangements we observe in our cryo-EM reconstruction, we used our atomic model to generate 3D densities representing each of the nucleotide states resolved by 2D analyses. These densities were then filtered to a resolution comparable to negative stain. 2D projections of the filtered substrate-bound  $^{\text{hex}}\text{YME1}^{\text{WB}}$  were consistent with the negative-stain 2D averages of this construct in the presence of ATP, serving as a positive control for these analyses (Fig. 3C, top row). The negative-stain data showed that two of the protomers were in different conformations from the other four subunits in the complex, consistent with the presence of three distinct nucleotide

states within our 3D structure (Fig. 3C, top row arrows). In contrast, our 2D analyses showed that all subunits in the apo and ADPAIF<sub>x</sub> samples adopted similar conformations within the hexamer, indicating that, in each case, the ATPases were in a homogeneous nucleotide state. The projections of the homohexamers generated from six copies of the ADP- and apo-like subunits revealed a structural organization that accurately reflects the ADPAIF<sub>x</sub>-bound and apo negative-stain 2D classes, respectively. Serving as further confirmation for these nucleotide-induced reorganizations, symmetric crystallographic structures of FtsH in the apo and ADP-bound state also resemble our apo- and ADP-like synthetic homohexamers (19, 20). Together, these data confirm the coexistence of three distinct nucleotide states in our substrate-bound structure and show that the nucleotide state is sufficient to induce major rotations of the ATPase subdomains in YME1. Moreover, our results strongly suggest that these nucleotide-dependent motions are required for the formation of the asymmetric spiral staircase configuration, because the subdomain movements induced by the ADP- and apo-like nucleotide states place these subunits in the lowermost and step positions, respectively.

### A hingelike glycine linker accommodates ATPase rearrangements above a flat protease ring

In this substrate-bound state, the movements of the ATPase subdomains do not involve a reorganization of the protease domains, which maintain a C6-symmetric planar organization (Fig. 1, A to C). As a result, the distance between the ATPase and protease domains is gradually reduced as the protomers progress around the ring (Fig. 1C and movie S1), which is further illustrated by distance matrices of the entire subunit (fig. S8B). The interdomain linker connecting the protease and ATPase domains of each protomer plays a crucial role in accommodating the ATPase domain motions while adhered to a planar protease ring. A glycine (G521) within the linker region is strictly conserved from bacteria to human and allows the hingelike motion of the small ATPase domain relative to the protease domain that gives rise to the different nucleotide states observed in our YME1 structure (Fig. 4B). Previous biochemical and structural studies of FtsH also highlighted the importance of this glycine for protease activity (19). To determine the structural and functional implications of this interdomain hinge for YME1 function, we mutated this glycine to a leucine to limit the possible backbone dihedral angles (G521L). Negative-stain EM analysis revealed that, regardless of the nucleotide state, the mutant construct always adopted an ADP-like conformation (compare Figs. 3C and 4C). Accordingly, this point mutation completely abolished YME1's ability to degrade the unfolded substrate T10-I27<sup>CD</sup> despite hydrolyzing ATP at ~70% of the wild-type rate (Fig. 4D and fig. S1B). This indicates that ATP hydrolysis is required, but not sufficient, for substrate processing, because ATPase domain rotations

enabled by the glycine linker are crucial for the translocation mechanism and ultimately proteolytic degradation.

### Positioning of the unfolded peptide in the protease domain enables processive degradation of the substrate

Our results show that the ATPase domain movements facilitate the translocation of an unfolded substrate peptide through the hydrophobic central pore into the hydrophilic chamber, where the protease domains comprise a negatively charged ring with all six cleavage sites facing the interior of the chamber (fig. S3A). The proteolytic active site of YME1 is well resolved in the reconstruction—a zinc ion is coordinated by two histidines (H540 and H544) and an aspartate (D618) (Fig. 1F) in an organization that is similar to that observed for other M41 proteases, such as the homologous FtsH (19–21). The active site is at the periphery of the protease ring in a small pocket that constitutes the only hydrophobic patch accessible from the interior of the chamber (fig. S3B). An antiparallel  $\beta$  strand is located directly adjacent to the proteolytic pocket, and we show that a 10-amino acid polyalanine un-

folded substrate peptide can interact with this  $\beta$  strand at the active site, precisely positioning it for proteolytic cleavage (fig. S3, C and D). The formation of interactions with the substrate polypeptide backbone atoms could enable sequence-independent cleavage, compatible with the degradation of the wide variety of YME1 substrates identified *in vivo* (35, 47–49).

### Model for the mechanism of action of YME1 and implications for other AAA+ unfoldases

We can use our data to define an ATP-dependent mechanism of substrate translocation by YME1. We show that the nucleotide state determines interprotomer coordination, ATPase subdomain motions, and pore loop conformation (Fig. 5, A and B). First, ATP hydrolysis in the lowermost ATP-bound subunit abolishes the interaction of the  $\gamma$ -phosphate with the trans-acting arginine finger residues from the clockwise adjacent subunit, thus releasing the bridging F411 and breaking the subunit-subunit interaction. This drives a major domain rotation that repositions this subunit in the lowermost register of the spiral staircase and weakens the interaction of its

pore loop tyrosines with the substrate. These motions then trigger ATP hydrolysis in the counterclockwise adjacent subunit, likely through subtle repositioning of the arginine fingers that are coordinating the neighboring ATP. Evidence of this coordination of nucleotide hydrolysis is seen in a study of YME1 paralogs, Yta10 and Yta12, which showed that ATP binding within a given subunit inhibits ATP hydrolysis in the counterclockwise adjacent subunit (44). As the counterclockwise subunit subsequently undergoes hydrolysis, its contacts with the triggering ADP-like subunit are lost, leaving the ADP-like subunit now untethered from both neighboring ATPase domains. The ADP-like subunit releases ADP, thereby transitioning to an apo-like step subunit state and completely breaking the interaction of the pore loops with the substrate. ATP binding by the apo step subunit reestablishes the interactions between the  $\gamma$ -phosphate and the trans-acting elements of its clockwise adjacent ATP-bound subunit to restore the spiral staircase arrangement, with the previous apo subunit now occupying the uppermost ATP-bound position. Iteration of this sequence of events leads to a sequential ATP hydrolysis cycle that proceeds

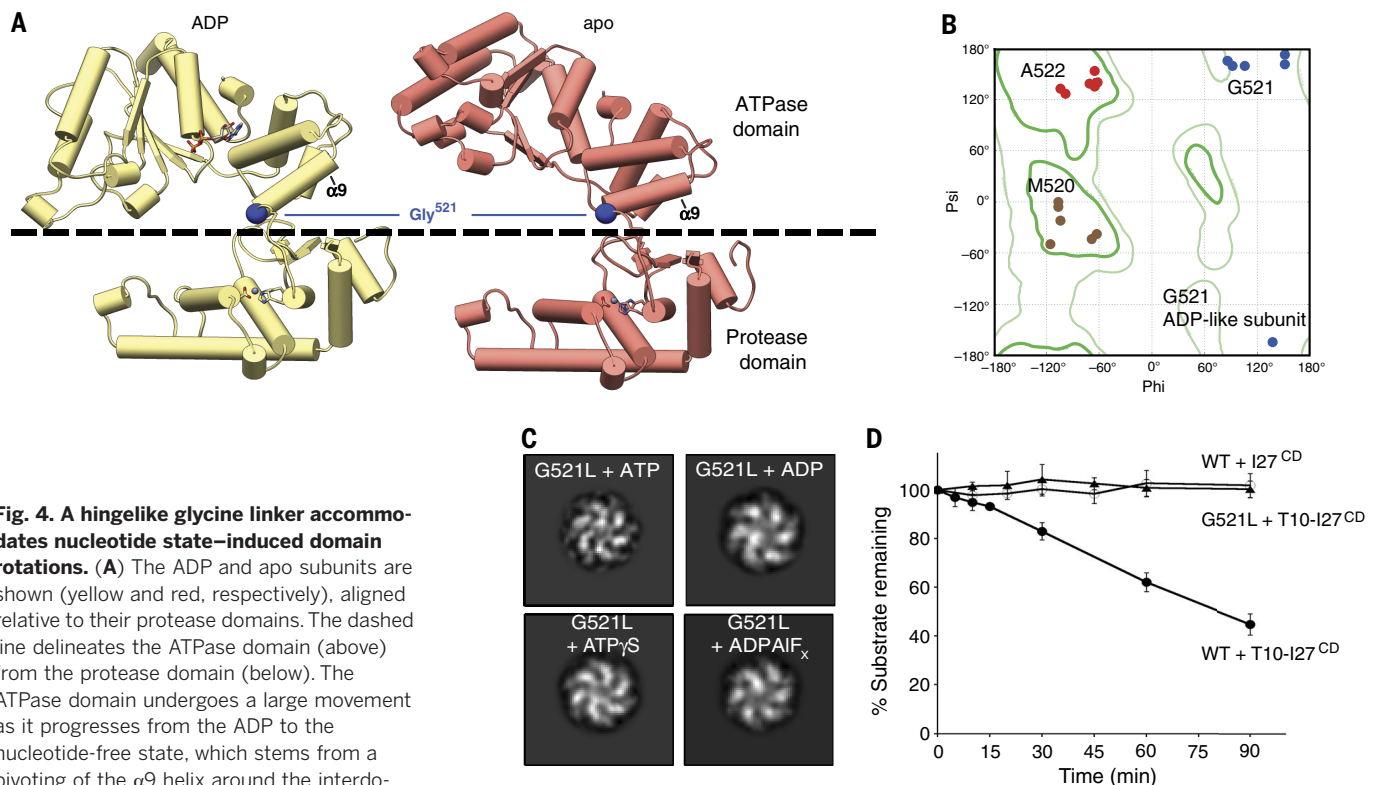


**Fig. 4. A hingelike glycine linker accommodates nucleotide state-induced domain rotations.**

(A) The ADP and apo subunits are shown (yellow and red, respectively), aligned relative to their protease domains. The dashed line delineates the ATPase domain (above) from the protease domain (below). The ATPase domain undergoes a large movement as it progresses from the ADP to the nucleotide-free state, which stems from a pivoting of the  $\alpha 9$  helix around the interdomain linker. G521 within this linker is shown to play a key role in enabling this large-scale motion. (B) Ramachandran plot displaying phi and psi angles of interdomain residues M520 (brown), G521 (blue), and A522 (red) in each subunit shows major torsion changes of G521 in the ADP-like state. The location of the G521 phi and psi angles underscores the necessity of a torsionally flexible Gly in this position. (C) 2D image analyses of a negatively stained <sup>hex</sup>YME1 construct containing a G521L mutation show that the addition of ATP, ADP, ADPAIF<sub>x</sub>, and ATP $\gamma$ S does not significantly influence the quaternary organization of the complex. Because all the

resulting class averages appear to have a similar organization as the ADP-like conformation shown in Fig. 3C, we suspect that the subunits of this mutant construct are trapped in the ADP conformation. (D) Plot showing the effect of the G521L mutation on the degradation of an unfolded substrate. Rapid loss of T10-I27<sup>CD</sup> is seen over time in the presence of WT <sup>hex</sup>YME1, whereas no loss of T10-I27<sup>CD</sup> is observed in the presence of the G521L point mutant or for unfolded I27<sup>CD</sup> lacking the T10 degron incubated with WT <sup>hex</sup>YME1. Values are means of independent replicates ( $n \geq 3$ )  $\pm$  SD.

around the ring in a counterclockwise manner (Fig. 5A). This sequential model is in agreement with mechanisms proposed for other AAA+ ATPases (23, 24, 28, 44, 50, 51).

This tightly coordinated ATP hydrolysis cycle and its allosteric relation to pore loop conformation enable a constant grip on the substrate as it is threaded through the central pore in a stepwise

manner (Fig. 5B). The ATP-bound subunits bind the substrate, whereas the ADP-bound subunit releases the substrate at the lowest position of the spiral, and the nucleotide-free subunit transitions to the highest position of the spiral staircase, where it reattaches to the substrate upon ATP binding (movies S1 and S3). The unfolded substrate is translocated in this fashion toward

the negatively charged proteolytic chamber, where it is positioned for cleavage at the zinc-coordinated active site of the planar protease domains. The large-scale motions of the ATPase closed spiral staircase observed in our structure are accommodated over a planar protease ring through a glycine residue within the linker connecting these domains.

### Concluding remarks

Our high-resolution structure of the soluble domains of a mitochondrial IM AAA+ protease provides a structural framework that explains decades of biochemical and genetic investigation of the activity and regulation of this class of unfoldase (36, 52). Furthermore, our asymmetric substrate-bound YME1 structure containing four ATP, one ADP-like, and one apo-like subunits is in agreement with previous biochemical data describing other unfoldases, including ClpX, PAN, and HslU, which showed a maximum of four ATP molecules and three co-existing functional subunit classes per hexamer (40, 53, 54). Our model for ATP-driven substrate translocation incorporates and explains a number of previously identified mechanistic features from a wide variety of AAA+ ATPases, including direct interactions of the aromatic pore loop residues with highly diverse substrates (29, 30, 34, 55, 56). We propose that the intercalation of pore loop tyrosines into the substrate polypeptide observed here is likely to be conserved across AAA+ unfoldases, because they enable substrate translocation independent of sequence. The presence of an additional tyrosine within the AAA+ staircase appears to be specific to YME1 (fig. S7A), suggesting that increased hydrophobicity of the central pore may have evolved to improve the enzyme's grip on greasy regions located within the numerous endogenous transmembrane substrates previously reported to be pulled out of the membrane by YME1 (44, 57, 58). Furthermore, the increased structural flexibility of YME1 oligomers observed in the absence of nucleotide, which results from the loss of intersubunit coordination, provides an explanation for the stress-induced proteolytic degradation of YME1L associated with reduced nucleotide levels that can affect recovery from ischemic reperfusion in mice (10–12). The atomic description of how the AAA+ ATPase domains engage substrates will guide future studies aimed at unveiling the mechanisms that endow mitochondrial IM AAA+ proteases to act either as site-specific proteases or through processive degradation, and thereby regulate mitochondrial activity and morphology. These mechanisms are likely to be conserved given the high sequence similarity of these quality control complexes (fig. S7A).

Recently solved substrate-bound structures of other AAA+ unfoldases have all revealed a staircase-like configuration of the ATPase subunits, leading to similar proposals for sequential nucleotide-driven translocation mechanisms (23, 24, 28). Although a degree of stochasticity cannot be excluded (for example, in the absence of the substrate or upon stalling of the enzyme),

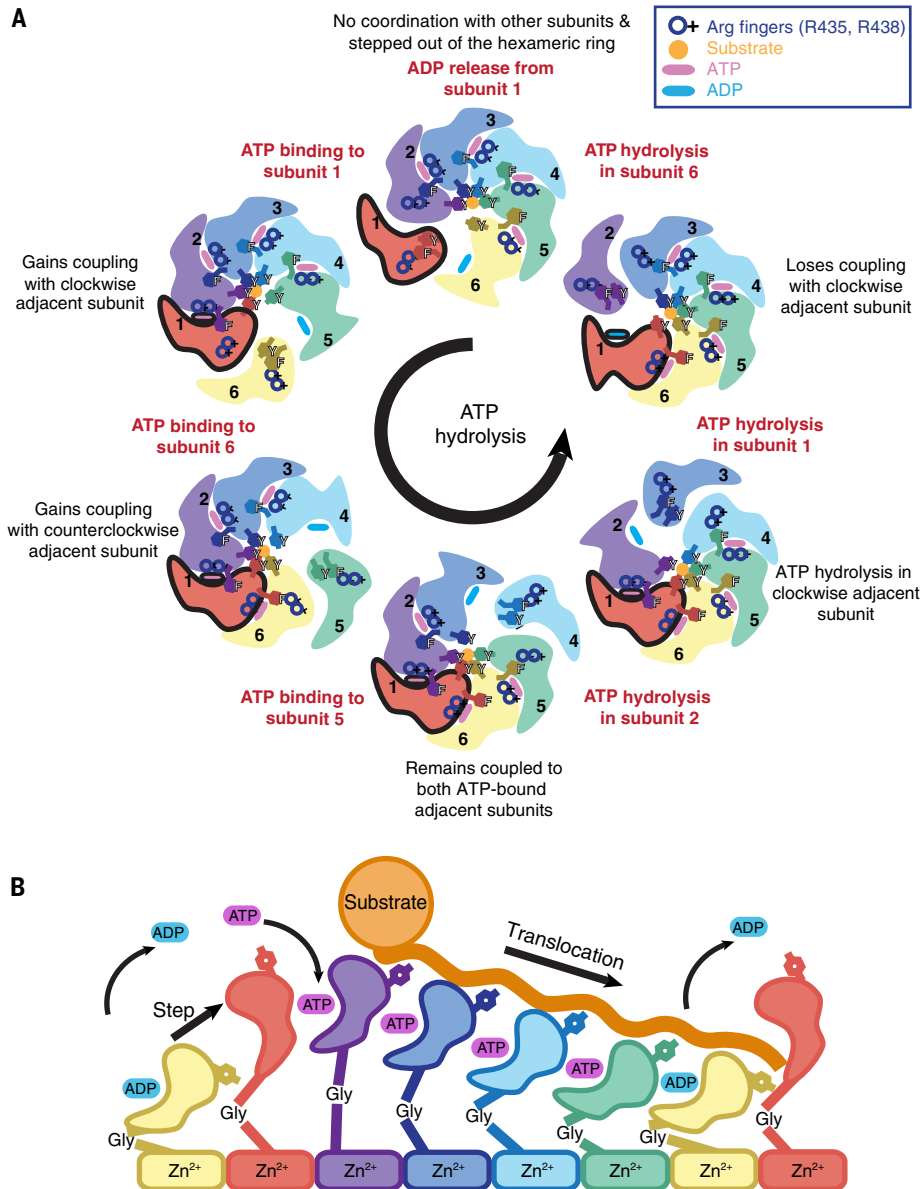


**Fig. 5. Putative model for ATP-driven substrate translocation into the proteolytic chamber of YME1.** (A) Cartoon representation of the putative ATP hydrolysis cycle that proceeds sequentially in a counterclockwise manner around the hexameric ATPase ring. We show how the coordinated nucleotide-dependent changes in the hexamer may affect the subunit shown in red throughout the cycle. ATP and ADP are represented as blue and pink ovals at the interprotomer interface, and an orange circle depicts the substrate trapped in the central pore and coordinated by the pore loops. (B) Putative scheme of the progressive conformational rearrangements of a given subunit as it progresses through a single ATP hydrolysis cycle (from left to right): ADP release, ATP binding, ATP-bound states, ATP hydrolysis, ADP state, and ADP release. Each nucleotide state is highlighted by a different color. The yellow and red subunits are shown twice to highlight the complete cycle.

the observed spiraling organization of the ATPase domains in this and other substrate-bound structures of AAA+ unfoldases (23, 24, 28) strongly supports a conserved, tightly coordinated ATP hydrolysis cycle as the main driver of AAA+ ATPase activity. Furthermore, we confirm that three coexisting nucleotide states give rise to the ATPase staircase. We propose that the mechanism of allostery coordinating the nucleotide state with substrate binding is conserved across other type I ATPases, including the AAA+ ATPases of the 26S proteasome, which share more than 35% sequence identity and show notable structural conservation of the closed spiral staircase configuration, as well as the key residues identified in YME1 (fig. S7, A and B). The marked structural similarity between a yeast mitochondrial ATPase and a functionally related human cytosolic ATPase suggests that our proposed hydrolysis and translocation mechanism may be conserved throughout eukaryotic unfoldases and could help explain many aspects of the 26S proteasome translocation mechanism, which, despite many high-resolution structures, remain unexplained (59).

## Materials and methods

### Cloning and purification

A plasmid containing <sup>hex</sup>YME1<sup>WB</sup> was generated as previously described (18). All additional variants of <sup>hex</sup>YME1 were generated by site-directed mutagenesis using wild-type <sup>hex</sup>YME1 as a template. All <sup>hex</sup>YME1 variants were expressed and purified as previously described (17, 18) with the following alterations. Proteins used in cryo-EM studies were buffer exchanged immediately prior to size exclusion chromatography into a buffer containing 20 mM Tris-HCl (pH 8.0), 300 mM NaCl, 2 mM EDTA, 10% glycerol, and 1 mM DTT. Proteins were then applied to a Superose 6 Increase column (GE Healthcare) pre-equilibrated in the same buffer. The peak corresponding to hexameric <sup>hex</sup>YME1 was pooled, and buffer exchanged into a buffer containing 20 mM Tris-HCl (pH 8.0), 300 mM NaCl, 15 mM MgCl<sub>2</sub>, 10% glycerol, and 1 mM DTT. Size exclusion was repeated using a Superose 6 increase column pre-equilibrated in a buffer containing 25 mM HEPES (pH 8.0), 100 mM KCl, 5% glycerol, 5 mM MgCl<sub>2</sub>, and 1 mM DTT. Fractions containing target proteins were pooled, concentrated and flash frozen prior to storage at -80°C.

Sequence encoding I27 and I27<sup>CD</sup> (18) were subcloned into a modified pET His6 SUMO vector (2S-U) (15) (2S-U-I27; 2S-U-I27<sup>CD</sup>) and the T10 degenon sequence was appended to the N-terminus of both constructs by PCR. All I27 variants were expressed in *E. coli* strain BL21-CodonPlus (Novagen) and purified as described for <sup>hex</sup>YME1 substrates (18).

### Biochemical assays

All ATPase and protein degradation assays were performed as previously described (18). ATPase assays were carried out at 30°C and contained 0.2 μM enzyme. Protein degradation reactions were carried out at 30°C and contained 20 μM

substrate, 0.5 μM enzyme, and 5 mM ATP regeneration system. Substrate degradation was visualized on 12% SDS-PAGE stained with Coomassie Blue R-250. Loss of full-length substrate band intensities were quantified using ImageJ (60) and initial degradation rates calculated from at least five time points in the linear range. All intensities were normalized to 100% full-length substrate at 0 seconds (61).

### Sample preparation for electron microscopy

For negative stain electron microscopy analysis of nucleotide induced conformational changes, 0.1 μM <sup>hex</sup>YME1 was incubated for 5 minutes on ice in 25 mM HEPES pH 8, 100 mM KCl, 5 mM MgCl<sub>2</sub>, 1 mM DTT in the absence or presence of nucleotide (1 mM ATP or ADPAIF<sub>x</sub>). After incubation, 4 μl of the sample were applied onto plasma cleaned 400 mesh Cu-Rh maxtaform grids (Electron Microscopy Sciences) coated with a thin layer of amorphous carbon. The grids were immediately stained with 2% (w/v) uranyl formate solution, and blotted to dryness.

After extensive cryo-EM screening to overcome strong preferred orientation, 0.76 mg/ml <sup>hex</sup>YME1<sup>WB</sup> was incubated on ice for 5 minutes in 25 mM HEPES pH 8, 100 mM KCl, 5 mM MgCl<sub>2</sub>, 1 mM DTT, 1 mM ATP and 0.05% Lauryl Maltose Neopentyl Glycol (LMNG, Anatrace). 3 μl of the sample were applied onto plasma cleaned UltraAuFoil Holey Gold Films R1.2/1.3, 300 mesh (Quantifoil) and immediately vitrified by plunge freezing in liquid ethane slurry at -180°C. The entire procedure was performed using Vitrobot (FEI) at 4°C and 100% humidity.

### Electron microscopy data acquisition

Negative-stain EM micrographs were collected on a Tecnai Spirit (FEI) transmission electron microscope operated at 120 kV with a Lab6 filament using the Legikon automated acquisition software (62). Images were collected using an F416 CMOS 4Kx4K-pixel camera (TVIPS) at a nominal magnification of 52000x and a pixel size of 2.05 Å/pixel at specimen level. For each condition, 100,000 particles were picked from approximately 200 micrographs with an electron dose of 20 e<sup>-</sup>/Å<sup>2</sup> using a defocus range of 0.5-1.5 μm.

Cryo-EM data were collected on a Titan Krios transmission electron microscope operating at 300 keV and micrographs were acquired using a Gatan K2 Summit direct electron detector, operated in electron counting mode applying a total dose of 60 e<sup>-</sup>/Å<sup>2</sup> as a 28-frame dose-fractionated movie during a 7 s exposure. Legikon data collection software was used to collect 6098 micrographs at 29,000x nominal magnification (1.026 Å/pixel at the specimen level) and nominal defocus range of -1.2 to -2.5 μm.

### Image processing

For all negative stain data, the contrast transfer function was determined with CTFFind4 (63) and particles were picked using Difference of Gaussians (DoG)-based automated particle picker

(64), both implemented in the Appion processing pipeline (65). Final stacks of approximately 100000 particles were generated using RELION 1.4 (66) at a 144x144 box size, binned by a factor of 2 for processing. 2D classes were obtained using Reference free 2D alignment in Relion 2.0, but attempts to generate a reliable 3D reconstruction failed for all states, with the exception of the ATP-bound state.

During cryo-EM data collection, micrograph frames were aligned using MotionCorr2 (67), implemented in the Appion workflow (65). CTF parameters were estimated with CTFFind4 (63) and only micrographs with confidence values above 95% were further processed. Particles were picked with the FindEM template-based particle picker (68), using the negative stain 2D classes as templates. An initial 2,285,499 particle stack was created using a 256 pixel box size, which was scaled down by a factor of 4 using RELION 1.4 (66). 2D classification of these particles was performed in RELION 2.0 (69), and only averages showing high resolution features were retained. The negative stain reconstruction was low pass filtered to 60 Å and used as an initial model for 3D refinement of 1,792,531 particles in RELION 2.0. The x & y shifts from this refinement were used to re-extract the centered, unbinned particles using a box size of 256 pixels. These particles refined to a reported resolution of 3.5 Å by FSC=0.143, but the resolution was severely anisotropic, and the reconstruction exhibited artifacts from preferred orientation. The particles from this reconstruction were then sorted by classification without alignment into five classes, two of which, accounting for 2% of particles each, displayed high-resolution features that did not display anisotropic resolution artifacts. The 62,917 particles from these classes were merged, refined, and post-processed to produce a final reconstruction with an estimated resolution of 3.4 Å by gold standard FSC at 0.143.

As the reconstruction from this subset of particles contained substrate density in the pore, we wondered if this density could be arising from self-degradation, as was observed for the VAT ATPase (24). We did not observe stacked rings in our raw micrographs (fig. S2A), and focused classification of the regions above or below the pore did not reveal any densities that were suggestive of auto-degradation. However, auto-degradation of YME1 cannot be ruled out as a possible source of this substrate density.

The cryo-EM density of the step subunit was poorly resolved in this reconstruction, so a soft edged 3D mask was generated to encompass the step subunit and used to “continue” the RELION refinement. Refinement of the masked step subunit improved the quality of the map in this region (fig. S2D), with a reported resolution of 3.7 Å by FSC at 0.143.

### Atomic model building and refinement

A homology model was generated using the structure of a subunit of FtsH as a starting point. This initial model was split into the small and large domains of the ATPases and the protease and



- EMBO J.* **26**, 325–335 (2007). doi: [10.1038/sj.emboj.7601514](https://doi.org/10.1038/sj.emboj.7601514); pmid: [17245427](https://pubmed.ncbi.nlm.nih.gov/17245427/)
58. K. Leonhard *et al.*, Membrane protein degradation by AAA proteases in mitochondria: Extraction of substrates from either membrane surface. *Mol. Cell* **5**, 629–638 (2000). doi: [10.1016/S1097-2765\(00\)80242-7](https://doi.org/10.1016/S1097-2765(00)80242-7); pmid: [10882099](https://pubmed.ncbi.nlm.nih.gov/10882099/)
59. L. Budenholzer, C. L. Cheng, Y. Li, M. Hochstrasser, Proteasome structure and assembly. *J. Mol. Biol.* [10.1016/j.jmb.2017.05.027](https://doi.org/10.1016/j.jmb.2017.05.027) (2017). doi: [10.1016/j.jmb.2017.05.027](https://doi.org/10.1016/j.jmb.2017.05.027); pmid: [28583440](https://pubmed.ncbi.nlm.nih.gov/28583440/)
60. C. A. Schneider, W. S. Rasband, K. W. Eliceiri, NIH Image to ImageJ: 25 years of image analysis. *Nat. Methods* **9**, 671–675 (2012).
61. E. Gur, M. Vishkautzan, R. T. Sauer, Protein unfolding and degradation by the AAA+ Lon protease. *Protein Sci.* **21**, 268–278 (2012). doi: [10.1002/pro.2013](https://doi.org/10.1002/pro.2013); pmid: [22162032](https://pubmed.ncbi.nlm.nih.gov/22162032/)
62. C. Suloway *et al.*, Automated molecular microscopy: The new Legation system. *J. Struct. Biol.* **151**, 41–60 (2005). doi: [10.1016/j.jsb.2005.03.010](https://doi.org/10.1016/j.jsb.2005.03.010); pmid: [15890530](https://pubmed.ncbi.nlm.nih.gov/15890530/)
63. A. Rohou, N. Grigorieff, CTFFIND4: Fast and accurate defocus estimation from electron micrographs. *J. Struct. Biol.* **192**, 216–221 (2015). doi: [10.1016/j.jsb.2015.08.008](https://doi.org/10.1016/j.jsb.2015.08.008); pmid: [26278980](https://pubmed.ncbi.nlm.nih.gov/26278980/)
64. N. R. Voss, C. K. Yoshioka, M. Radermacher, C. S. Potter, B. Carragher, DoG Picker and TiltPicker: Software tools to facilitate particle selection in single particle electron microscopy. *J. Struct. Biol.* **166**, 205–213 (2009). doi: [10.1016/j.jsb.2009.01.004](https://doi.org/10.1016/j.jsb.2009.01.004); pmid: [19374019](https://pubmed.ncbi.nlm.nih.gov/19374019/)
65. G. C. Lander *et al.*, Appion: An integrated, database-driven pipeline to facilitate EM image processing. *J. Struct. Biol.* **166**, 95–102 (2009). doi: [10.1016/j.jsb.2009.01.002](https://doi.org/10.1016/j.jsb.2009.01.002); pmid: [19263523](https://pubmed.ncbi.nlm.nih.gov/19263523/)
66. S. H. W. Scheres, RELION: Implementation of a Bayesian approach to cryo-EM structure determination. *J. Struct. Biol.* **180**, 519–530 (2012). doi: [10.1016/j.jsb.2012.09.006](https://doi.org/10.1016/j.jsb.2012.09.006); pmid: [23000701](https://pubmed.ncbi.nlm.nih.gov/23000701/)
67. S. Q. Zheng *et al.*, MotionCor2: Anisotropic correction of beam-induced motion for improved cryo-electron microscopy. *Nat. Methods* **14**, 331–332 (2017). doi: [10.1038/nmeth.4193](https://doi.org/10.1038/nmeth.4193); pmid: [28250466](https://pubmed.ncbi.nlm.nih.gov/28250466/)
68. A. M. Roseman, FindEM—A fast, efficient program for automatic selection of particles from electron micrographs. *J. Struct. Biol.* **145**, 91–99 (2004). doi: [10.1016/j.jsb.2003.11.007](https://doi.org/10.1016/j.jsb.2003.11.007); pmid: [15065677](https://pubmed.ncbi.nlm.nih.gov/15065677/)
69. D. Kimanius, B. O. Forsberg, S. H. W. Scheres, E. Lindahl, Accelerated cryo-EM structure determination with parallelisation using GPUs in RELION-2. *eLife* **5**, e18722 (2016). doi: [10.7554/eLife.18722](https://doi.org/10.7554/eLife.18722); pmid: [27845625](https://pubmed.ncbi.nlm.nih.gov/27845625/)
70. M. A. Herzik Jr., J. S. Fraser, G. C. Lander, A multi-model approach to assessing local and global cryo-EM map quality. *bioRxiv* (2017). doi: [10.1101/128561](https://doi.org/10.1101/128561)

#### ACKNOWLEDGMENTS

We thank J.-C. Ducom at The Scripps Research Institute High Performance Computing for computational support and B. Anderson at The Scripps Research Institute electron microscopy facility for microscope support. We thank B. Ding for helpful discussions on sample preparation and M. Herzik and S. Chowdhury for helpful discussions and training in data collection and atomic modeling. C.P. is supported by

an American Heart Association predoctoral fellowship. G.C.L. is supported as a Searle Scholar and a Pew Scholar and by NIH grant DP2EB020402. Computational analyses of EM data were performed using shared instrumentation funded by NIH grant S100D021634 (to G.C.L.). A.J.R. was supported by NIH training grant T32GM008468. A.J.R. and S.E.G. are supported by NIH grant R01GM115898. R.L.W. is supported by NIH grant R01NS095892. EM maps, including sharpened, unsharpened, focused classification of the step subunit, and all associated half maps, are deposited to the Electron Microscopy Data Bank under accession number EMD-7023. Five atomic models that equally represent the EM density have been deposited as a multimodel entry at the Protein Data Bank under accession number PDB ID: 6AZ0. C.P. performed all cryo-EM structure determination, model building and refinement, and mechanistic interpretation and wrote the manuscript. C.P. and M.S. performed the negative-stain EM experiments. A.J.R. and C.J.G. created all constructs and purified proteins. A.J.R. performed all biochemical experiments. All authors contributed to the experimental design and editing of the manuscript.

#### SUPPLEMENTARY MATERIALS

[www.sciencemag.org/content/358/6363/eaao0464/suppl/DC1](http://www.sciencemag.org/content/358/6363/eaao0464/suppl/DC1)  
Figs. S1 to S8  
Table S1  
Movies S1 to S3  
References (71–74)

26 June 2017; accepted 25 September 2017  
10.1126/science.aao0464

## Structure of the mitochondrial inner membrane AAA+ protease YME1 gives insight into substrate processing

Cristina Puchades, Anthony J. Rampello, Mia Shin, Christopher J. Giuliano, R. Luke Wiseman, Steven E. Glynn and Gabriel C. Lander

*Science* **358** (6363), eaao0464.  
DOI: 10.1126/science.aao0464

### Feeding a protease step by step

Proteins that degrade damaged or misfolded mitochondrial proteins are essential for mitochondrial function. A key player is the hexameric protease YME1, in which each subunit is anchored in the inner mitochondrial membrane by a helix and has an adenosine triphosphatase (ATPase) domain and a protease domain in the intermembrane space. Puchades *et al.* report a high-resolution structure that shows that the ATPase domains form an asymmetric spiral staircase that stacks above a planar protease ring. Conserved tyrosine residues in the central pore of the spiral staircase interact with a substrate peptide. The ATP hydrolysis cycle is sequential and coordinated with changes in the position of the tyrosine residues that result in stepwise translocation of the substrate into the protease chamber.

*Science*, this issue p. eaao0464

#### ARTICLE TOOLS

<http://science.sciencemag.org/content/358/6363/eaao0464>

#### SUPPLEMENTARY MATERIALS

<http://science.sciencemag.org/content/suppl/2017/11/02/358.6363.eaao0464.DC1>

#### REFERENCES

This article cites 74 articles, 14 of which you can access for free  
<http://science.sciencemag.org/content/358/6363/eaao0464#BIBL>

#### PERMISSIONS

<http://www.sciencemag.org/help/reprints-and-permissions>

Use of this article is subject to the [Terms of Service](#)